Compressive Behaviour of Concrete Cylinders Reinforced with Glass Fiber Reinforced Polymer Bars

Fillmore, Brandon[1] and Sadeghian, Pedram[1,2]

[1] Department of Civil and Resource Engineering, Dalhousie University, 1360 Barrington Street, Halifax, NS B3H 4R2, Canada

[2] pedram.sadeghain@dal.ca

Abstract: Current design standards ignore any contribution of glass fiber reinforced polymer (GFRP) bars in concrete in a state of compression. This paper challenged this convention by testing 30 cylinders of 36 MPa concrete to failure in pure axial compression. The testing matrix consisted of control groups of plain and steel-reinforced concrete specimens which were used to benchmark groups of concrete specimens reinforced with commercial and modified GFRP bars. Cylinders were built in 4, 6, and 8 bar arrangements with nominal diameters of 10M or 13M and with concrete cover 25 mm, cylinder diameter 150 mm and height 300 mm. The GFRP bars were found to exhibit crushing failure long after the concrete in the cylinders had been crushed. Commercial GFRP bars significantly increase the toughness of the specimens over unreinforced concrete, outperforming both steel and modified GFRP reinforcement in this metric. However, steel reinforcement proved to increase peak load the most over unreinforced concrete, with commercial and modified GFRP reinforcement increasing peak load by less than half as much as steel.

1   Introduction

The use of glass fiber-reinforced polymer (GFRP) bars for reinforcing concrete structures has been significantly grown during the past three decades. The corrosion resistance nature of GFRP bars against de-icing salt, ocean water, and other harsh environments has been the main advantage over steel bars. Moreover, GFRP bars' high strength, light weight, and reasonable cost have been other advantages. The application of GFRP bars in concrete beams and slabs has been relatively established (Benmokrane et al. 1995 and El-Sayed et al. 2005). However, the use of GFRP bars in concrete columns has been very limited.

Despite experimental studies demonstrating significant contribution of GFRP bars in concrete columns (De Luca et al. 2010 and Tobbi et al. 2012), design guidelines (e.g. ACI 440.1R 2015 and CAN/CSA S806-12. 2012) for GFRP bars currently neglects their contribution in compression. It means further research is needed into the application of GFRP reinforced concrete members in compressive applications is needed to establish a definite understanding of their use.

The current design approach of neglecting any GFRP bar compressive contribution is rooted in concerns surrounding the micro-buckling of the anisotropic bars (De Luca et al. 2010). The objective of this research is to examine how GFRP bars behave under compressive loading in short GFRP reinforced concrete cylinders. Within the cylinders, variations in the number of GFRP bars allows for a thorough examination of their compressive behaviour compared with steel-reinforced and unreinforced concrete cylinders.

2 Experimental Program

2.1 Specimen Layout

A total of 30 concrete cylinders with a diameter of 150 mm and a height of 300 mm were prepared and tested under uniaxial compression loading. The testing matrix consisted of control groups of plain and steel-reinforced concrete specimens which were used to benchmark groups of concrete specimens reinforced with commercial and modified GFRP bars. Cylinders were built in 4, 6, and 8 bar arrangements with nominal diameters of 10 and 13 mm. Table 1 shows the test matrix. Three identical specimens per group were prepared and tested.

Table 1: Test matrix

ID #	Specimen group	Reinforcement type	Bar dimension	Number of bars
1	Plain	-	-	-
2	Steel 4-Bar	Steel	10M	4
3	Steel 6-Bar	Steel	10M	6
4	Steel 8-Bar	Steel	10M	8
5	C GFRP 4-Bar	GFRP	13M	4
6	C GFRP 6-Bar	GFRP	13M	6
7	C GFRP 8-Bar	GFRP	13M	8
8	M GFRP 4-Bar	GFRP	10M	4
9	M GFRP 6-Bar	GFRP	10M	6
10	M GFRP 8-Bar	GFRP	10M	8

2.2 Material Properties

Concrete slurry was delivered in a ready mix batch with maximum aggregate size of 13 mm. The average compressive strength of concrete at the time of test was 36 MPa. The manufacturer's specifications for the 13M commercial GFRP bars are for a nominal area of 126.7 mm^2 with the tensile properties of peak load, ultimate strength, and elastic modulus being specified as 95.90 kN, 758 MPa and 46 GPa, respectively. Similarly, the modified GFRP bars were sourced from 10M commercial GFRP bars from the same manufacturer and the modifications are presently being assumed to have had negligible effect on the geometric and mechanical properties of the 10M bars, as-produced by the manufacturer. The 10M GFRP bars as-produced by the manufacturer were specified to have a nominal area of 71.26 mm^2, with the tensile properties of peak load, ultimate strength and elastic modulus being specified as 58.72 kN, 827 MPa and 46 GPa, respectively. The steel bars used were 10M with a specified tensile strength of 400 MPa and an elastic modulus of 200 GPa.

2.3 Specimen Preparation

The dimensions and compressive testing procedure followed the ASTM (ASTM C39M-16, 2016) but with specimen-construction modifications to accommodate and isolate the effects of the GFRP and steel reinforcement. As shown in Figure 1, The reinforcing bars were radially located at equal angles about the centreline of the specimen, such that concrete cover was consistently 25 mm and the clear space between bars was at least 20 mm. Since alignment of the reinforcing was crucial to achieving consistent and meaningful data, a method of specimen preparation was developed to maintain the integrity of the reinforcement geometry throughout the building process.

Cylindrical plastic molds were modified to accommodate the reinforcement. Limited space within the 150x300mm specimen size lead to the development of a method whereby the bars would be end-bearing and keep precise longitudinal orientation without the use of internal ties: this was done by creating a temporary base beneath the mold to support the extruded ends of the bars during consolidation. The base functioned as cantilever, holding the bars in place using a rigid polymer-fine aggregate mixture. While the bonding mixture cured in the cantilever base, the bars were braced for proper alignment. This method

allowed the faces of the consolidated concrete specimens to be ground smooth such that specimens were able to be axially loaded through a uniform cross section. The cantilever base also proved to be sufficiently strong to maintain the reinforcement alignment during placement and consolidation of the concrete slurry. The slurry was placed and consolidated in two layers using scoops, a vibration table and then the surface was carefully troweled smooth. The consolidated concrete was left in the molds and covered to moist cure for 4 days before the molds were removed and the specimens were relocated to the laboratory.

2.4   Test Setup and Instrumentation

As shown in Figure 1, deformation of the specimens was measured using three linear variable differential transformer (LVDT) units fixed to the cylinder using a point-bearing yolk: two longitudinal LVDT units with 200mm gauge lengths were placed on polar opposite sides to measure axial strain while the third measured lateral deformation across the full 150mm diameter until spalling occurred. The reinforced specimens also implemented two 12mm longitudinal strain gauges each, which were bonded to flat surfaces machined in-house into the outward facing sides of the bars. The strain gauges were also protected by a protective coating and covered with aluminum tape. In each reinforced specimen, the two bars with strain gauges were placed in a similar polar opposite arrangement to the longitudinal LVDT units, with the strain gauges facing the outside of the specimens. The compressive testing was done on a 2 MN Instron test frame and was programmed to deform the specimens at a rate of 0.6 mm per minute. The specimens were compressed until either the internal reinforcement began to crush or until it did not seem safe to deform the specimen any further.

Figure 1: Specimen preparation and test set-up

3   Results and Discussion

3.1   Failure Mode

The control group of plain unreinforced concrete specimens all failed along a shear plane, and some light tapping with a hammer revealed that fractures were developed all around upper and lower shear cones. Both the 4 and 6 bar steel-reinforced specimens exhibited relatively ductile post peak behaviour, and every specimen in the steel reinforced group exhibited steel yielding and an audible fracturing in the concrete with longitudinal surface cracks approaching failure. After the specimens were removed from the testing frame, it became clear that the steel reinforcing separated a confined concrete core from the exterior concrete which ultimately spalled as shown in Figure 2. The concrete fracturing in most of the steel specimens resembled the conical failure of the plain concrete specimens but with the core being protected, except for the 4 bar steel reinforced specimens, where the shear cone permeated the perimeter of the core defined by the reinforcement bars.

The post peak behaviour of the 4 bar steel reinforced specimens consisted of two stages: the first a more sudden decline from peak load capacity and the second more gradual until the specimen effectively stopped resisting further deformation. Most of the 4, 6 and 8 bar steel-reinforced specimens were able to safely be tested until the steel reinforcement gave out and the concrete core was crushed. Upon the removal of the spalled concrete around the exterior of the specimens, the steel bars that gave out were locally buckled in the outward direction from the core. The 6 bar steel specimens consistently achieved high loads and its load resistance gradual tapered off with further deformation until the specimens resisted approximately half of the peak load, after which the specimens effectively ruptured. The 6 bar specimens did not have defined phases of load deformation failure like the 4 bar specimens. The steel in the 8 bar specimens dictated the specimen behaviour more than the 4 and 6 bar arrangements, which resulted in greater stiffness in exchange for comparatively premature rupture, post-peak.

Figure 2: Typical failure mode of specimens reinforced with steel (left) and GFRP (right) bars

The commercial GFRP reinforced specimens had similar intragroup trends for 4, 6 and 8 bar arrangements to that of the steel group. Since the commercial GFRP bars have greater diameter than that of steel, the difference in the behaviour of the 8 commercial GFRP bar reinforced specimens to the 4 and 6 bar arrangements is more profound than in the steel group. Using the 6 bar geometries for comparison, 6 bar steel reinforcement greatly increased the peak load and resulted in ductile behaviour as the steel yielded and concrete fractured; whereas the 6 bar commercial GFRP reinforcement resulted in a lower increase in peak load but with a much broader peak in the load deformation curve. The 6 bar GFRP reinforced concrete composite effectively cancelled the independent brittle failure modes of its components and resulted in a ductile failure mode, albeit with much less of an increase in the peak load compared to a similar steel specimen.

The modified GFRP bar reinforced specimens do not follow the exact same intragroup trends for 4, 6 and 8 bar arrangements because they are much smaller in effective area than the commercial GFRP bars. As a result, the 8 bar specimens did not undergo the same premature failure as in the other testing groups and instead the 8 bar arrangement was tougher than the 6 bar arrangement with only a 14kN reduction in peak load. The modified GFRP bars are designed to increase the elastic modulus of the bars to better resemble the early rigidity of steel reinforcement, but this was not determined since the bar diameter and reinforcement ratio within this group do not allow for a direct comparison as was done for the steel and commercial GFRP reinforced groups.

Table 2: Summarized results by group and reinforcement

ID #	Group	Peak load (kN)		Strain at peak load (mm/mm)		Toughness (kN-mm)	
		Average	SD	Average	SD	Average	SD
1	Plain	639.0	29.9	0.00210	0.00035	257.2	70.8
2	Steel 4-Bar	792.1	4.0	0.00255	0.00011	439.2	14.2
3	Steel 6-Bar	858.0	16.1	0.00292	0.00046	550.0	130.5
4	Steel 8-Bar	911.1	7.6	0.00240	0.00022	407.6	215.9
5	C GFRP 4-Bar	709.3	15.0	0.00255	0.00008	440.0	167.4
6	C GFRP 6-Bar	724.7	14.4	0.00325	0.00057	619.8	163.3
7	C GFRP 8-Bar	722.7	25.3	0.00202	0.00065	260.2	169.6
8	M GFRP 4-Bar	677.4	11.1	0.00244	0.00042	264.6	120.1
9	M GFRP 6-Bar	695.8	7.4	0.00247	0.00031	421.8	99.9
10	M GFRP 8-Bar	671.8	33.0	0.00305	0.00025	445.2	58.8

Note: SD = standard deviation

3.2 Effect of Bars on Peak Load

The steel reinforcement proved to have the greatest effect in increasing the peak load of the cylinders. The 4 bar steel arrangement increased the peak load over unreinforced concrete from 639 kN to 792 kN, and further increases of nearly 50 kN were made with the 6 bar arrangement and again with 8 bars. The 6 bar specimens essentially just continued to deform at a similar modulus to the 4 bar steel reinforced specimens to reach a higher load, but the 8 bar steel reinforced specimens proved to be much more influenced by the stiffness of steel: reaching the peak load early at a strain of 0.0024 mm/mm whereas peak load occurred at 0.0026 mm/mm and 0.0029 mm/mm for 4 and 6 bar arrangements, respectively. The increase in peak load over unreinforced concrete was much smaller in both the commercial and modified GFRP bar reinforced specimens. The peak load and strain-at-peak for all the groups are shown in Figure 3(a) and 3(b), respectively. In the figures, the error bars illustrate the sample standard deviations.

3.3 Effect of Bars on Modulus of Toughness

An important distinction between the 8 bar steel reinforced specimens and those with fewer bars is that the steel properties begin to dictate the stiffness of the specimens. The 8 bar specimens achieved the highest peak loads within the steel group, but the increased stiffness of the specimens came at a price as the high reinforcement ratio led to sudden brittle failure prematurely post peak. Since the radial distance of the bars is constant throughout all reinforced specimens, the 8 bar reinforcement geometry decreases the concrete-to-concrete bonding area between the confined core and the cover; which meant that the cover was prone to spalling with transverse expansion through the Poisson effect. As a result, the 8 bar specimens proved to have a lower modulus of toughness than even the 4 bar steel reinforced specimens. The 6 bar specimens essentially just continued to deform at a similar modulus to the 4 bar steel reinforced specimens to reach a higher load before proceeding to fail in the anticipated ductile manner. These results suggest that there is an optimization of the reinforcement ratio in order to achieve the maximum toughness in steel reinforced cylindrical columns.

Since the 46 GPa elastic modulus of the GFRP bars is much lower than the 200 GPa value for steel, the concrete begins to fracture before the commercial GFRP bars take full effect. Since GFRP itself is linear elastic until rupture at a high strain, this means that the commercial GFRP bar contribution consistently increases until the composite specimen relies almost entirely on the GFRP bars buried within fractured concrete. As previously mentioned, the composite behaviour of GFRP reinforcement bars in concrete can be optimized to exhibit consistent ductile failure post peak. The 6 bar GFRP reinforced specimens proved to have the highest modulus of toughness within the experiment at a value of 620 kN-mm, followed by 6 bar steel at 550 kN-mm and 8 bar modified GFRP at 445 kN-mm. The computed values for the modulus of toughness are shown in Figure 3(c).
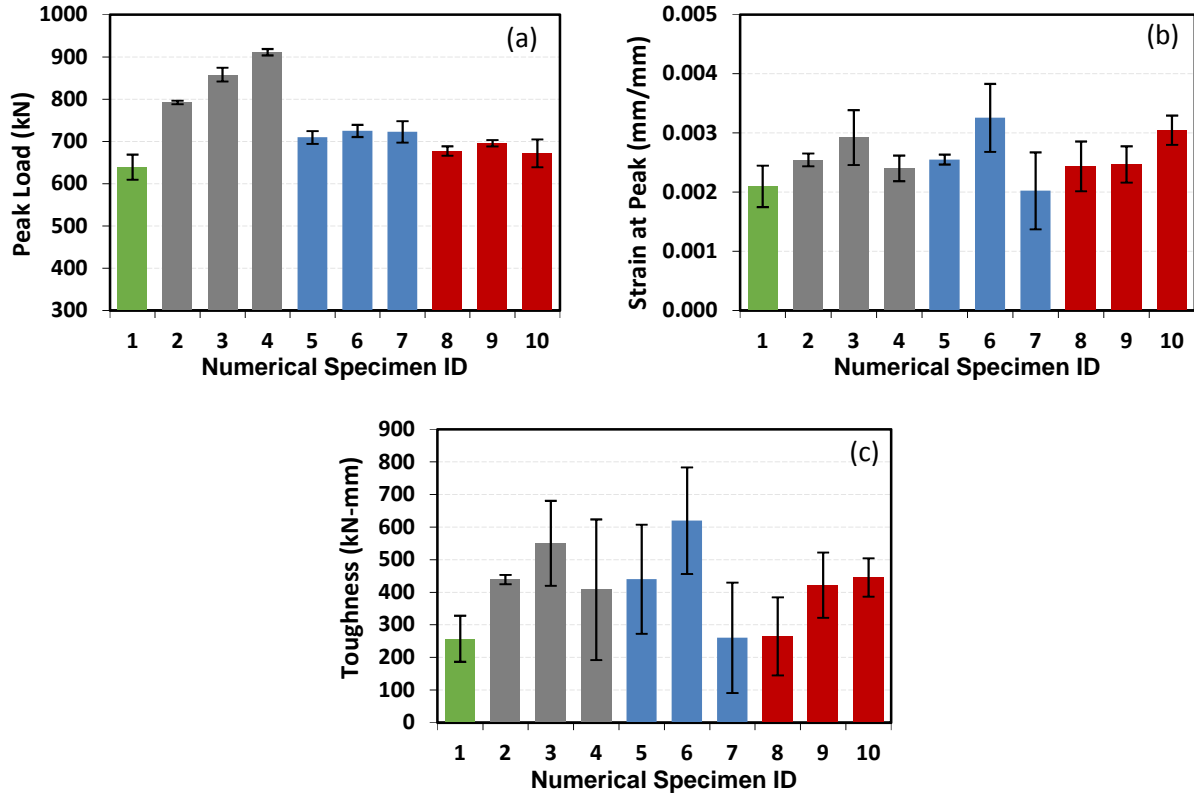
Figure 3: Variation of test results: (a) peak load; (b) strain at peak load; and (c) toughness. (see Table 1 for numerical specimen ID)

3.4 Load-Strain Behaviour

The effect of the bars which was discussed in sections 3.1 to 3.3 can be clearly seen in the representative load-strain curves comprising Figure 4, below. The high strain-at-peak-load of the GFRP bars themselves often resulted in a large plateau in the specimen's load resistance until one of the embedded bars ruptured. The toughness was computed by ending the numerical integration when a specimens' load resistance decreased to 85% of its peak load, so the long plateaus in the GFRP specimens do not affect the toughness values previously presented in Table 2. However, they are still meaningful in understanding the composite behaviour of GFRP reinforced concrete.
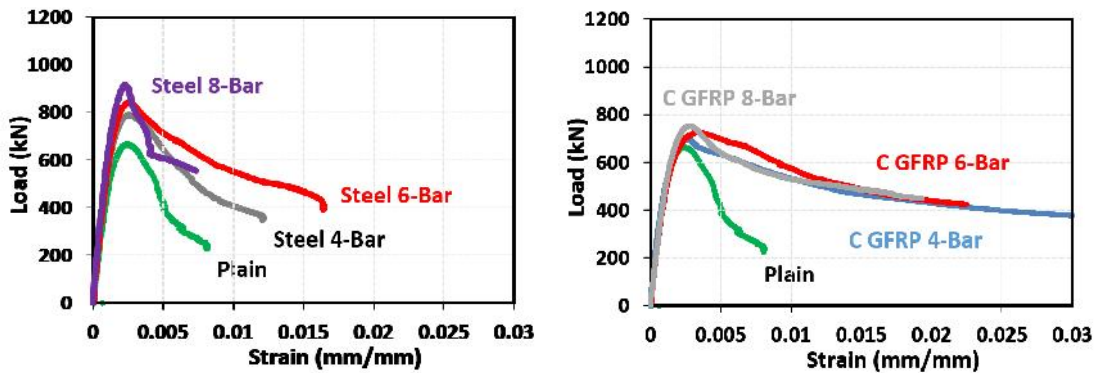

Figure 4: Typical load-strain curves

3.5   Bars Contribution at Peak Load

For each type of reinforcing bar used there were similar trends within each group as the number of bars was increased. The load strain behaviour up to the peak of the curve depends on the elastic modulus and reinforcement ratio. Thus, a normalized reinforcement ratio (ρ_n) for FRP-reinforced specimens was defined by multiplying the FRP reinforcement ratio (ρ_f) by the ratio of the elastic modulus of FRP reinforcement (E_f) to the elastic modulus of steel reinforcements (E_s) as follows:

$$[1] \quad \rho_n = \rho_f \frac{E_f}{E_s}$$

Two methods were used to determine the bars contribution at peak and these values were averaged. The first was the force method which uses the difference between the observed load resistance of a specimen and that which is predicted by the crushing strength of concrete and the area of concrete in the cross section of the sample. The second method employs the elastic modulus of the bars and the strain at peak load. The bar contribution at peak load of the specimens tested in this study are shown in Figure 5. It observed that the bar contribution at peak is directly proportional to the normalized reinforcement ratio.

For comparison, as shown in Figure 5, data from this current study was plotted alongside two other independent experimental studies by De Luca et al. (2010) and Tobbi et al. (2012), which analyzed compressive behaviour of GFRP reinforcement alongside conventional steel reinforced concrete. This external data also fit the linear relationship that was found in the current study. This is an ongoing research and more results will be presented at the time of the conference.
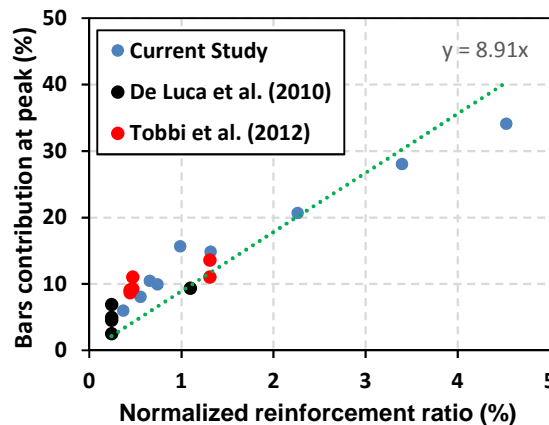

Figure 5: Bars contribution at peak vs normalized reinforcement ratio of this study compared to De Luca et al. (2010) and Tobbi et al. (2012)

4   Conclusions

In this study the effect of GFRP bars on the behaviour of axially loaded concrete cylinders was examined and benchmarked to steel reinforced and unreinforced control groups. The following conclusions can be drawn:

- By varying the number of bars for each type of reinforcement bar, data consistently demonstrated that an optimization function exists based on the reinforcement ratio of both GFRP and steel bars, which dictates their behaviour and allows for an insightful comparison of the reinforcement materials. Below the hypothetical optimum reinforcement ratio, shear failure was observed as the dominant failure mode. Above this hypothetical optimum, spalling of the concrete cover was observed with very distinct brittle failure of the specimens with further deformation beyond peak

load. The specimen groups nearest to this hypothetical optimum are Steel 6-Bar, C GFRP 6-Bar and M GFRP 8-Bar. Since the M GFRP group bars are much smaller in area than the C GFRP bars, none of the M GFRP Bar groups saw the same form of brittle failure from exceeding an optimum reinforcement ratio.

- The reinforcing bars contribution at peak load is a function of the reinforcement ratio and the elastic modulus of the bars. When the reinforcement ratio is normalized by multiplying it by the ratio of the elastic modulus of the reinforcement to that of conventional steel reinforcement, the bars contribution at peak was found to be a linear function.

- The ACI design guide for GFRP bars used in concrete reinforcement neglects the contribution of GFRP bars, but the results of this study show that GFRP bars have an appreciable effect on the peak load resistance of concrete in uniaxial compression. The C GFRP 6-Bar and M GFRP 6-Bar groups showed an increase in mean peak load by 86 kN and 57 kN beyond the Plain peak load of 639 kN. In comparison, the mean effect of steel in the Steel 6-Bar group showed a much larger increase in peak load beyond the Plain group of 219 kN.

- C GFRP bars were found to outperform steel, and M GFRP bars were found to be comparable to steel in terms of specimen toughness. While steel reinforced cylinders reached higher peak loads, GFRP reinforced specimens maintained a load resistance near their peak value through more deformation. The toughness values from the specimens nearest their hypothetical reinforcement ratios were found to be 550 kN-mm for Steel 6-Bar, 620 kN-mm for C GFRP 6-Bar and 445 kN-mm for M GFRP 8-Bar. In comparison, Plain specimens had a mean toughness of 257 kN-mm. These values demonstrate that GFRP bar reinforced concrete can be designed to exhibit high deformability.

5   Acknowledgements

6   References

ACI 440.1R.2015. Guide for the Design and Construction of Structural Concrete Reinforced with Fiber-Reinforced Polymer (FRP) Bars, American Concrete Institute.

ASTM C39M-16. 2016. Standard Test Method for Compressive Strength of Cylindrical Concrete Specimens, American Society of Testing and Materials.

Benmokrane, B., Chaallal, O. and Masmoudi, R., 1995. Glass fibre reinforced plastic (GFRP) rebars for concrete structures. Construction and Building Materials, 9(6), 353-364.

CAN/CSA S806-12. 2012. Design and Construction of Building Structures with Fibre-Reinforced Polymers. Canadian Standards Association.

El-Sayed, A., El-Salakawy, E. and Benmokrane, B., 2005. Shear strength of one-way concrete slabs reinforced with fiber-reinforced polymer composite bars. Journal of Composites for Construction, 9(2), pp.147-157.

De Luca, A., Matta, F. and Nanni, A. 2010. Behavior of Full-Scale Glass Fiber-Reinforced Polymer Reinforced Concrete Columns under Axial Load. ACI Structural Journal, 107(5): 589-596.

Tobbi, H., Farghaly, A.S. and Benmokrane, B. 2012. Concrete Columns Reinforced Longitudinally and Transversally with Glass Fiber-Reinforced Polymer Bars. ACI Structural Journal, 109(4): 551-558.